



CrossMark
 click for updates

Cite this: *RSC Adv.*, 2016, 6, 39144

Received 19th February 2016
 Accepted 13th April 2016

DOI: 10.1039/c6ra04444a

www.rsc.org/advances

Gold nanorods coated by oxygen-deficient TiO₂ as an advanced photocatalyst for hydrogen evolution†

S. F. Kou,^a W. Ye,^b X. Guo,^a X. F. Xu,^a H. Y. Sun^a and J. Yang^{*a}

Gold nanorods coated by oxygen-deficient TiO₂ are synthesized by slow hydrolysis followed with high-temperature annealing in a reducing atmosphere. This does not alter the morphology of the nanorods, but produces Ti³⁺ species and oxygen vacancies in the shell. These nanorods show superior photocatalytic ability in hydrogen generation. The enhanced performance may be attributed to the synergistic effect of Ti³⁺ species, oxygen vacancies and Au, which effectively enhance light absorption, reduce charge recombination and increase charge-transfer across the interface between the electrolyte and electrode.

TiO₂ as an important semiconductor for photovoltaics,¹ solar cells,² photocatalysis,^{3–5} and lithium ion batteries^{6–8} has been well explored in the past few decades, due to its high abundance, good chemical stability and low toxicity. However, as far as the photo-driven applications are concerned, the wide band gap of TiO₂, typically 3.0–3.4 eV, greatly limits its performances. Thus, various strategies like sensitizing with organic dyes or narrow band-gap semiconductors,^{9–12} coupling with metal nano-particles,^{13–16} and heterogeneous doping by metals or non-metals,^{17–19} have been successfully developed to extend the light absorption to the visible and near-infrared regions. Recently, a new strategy based on self-doping of Ti³⁺ accompanied by the formation of oxygen vacancies has been reported to improve the photo-driven performances of TiO₂, including degradation of organic molecules, water splitting, *etc.*^{20–25} The enhanced performances are attributed to the reduced band gap, the increased

charge carriers, and electron conductivity caused by Ti³⁺ and oxygen vacancies.

Combination of the strategy which introduces Ti³⁺ with the others like metal-decoration is an effective way to maximize the photo-catalytic performances of TiO₂. However, this attempt is scarcely reported yet, to the best of our knowledge. Xu's group deposited metallic gold nanoparticles on the surface of oxygen-vacancy-rich TiO₂, and reported the enhanced photo-activity and excellent photo-stability toward dye degradation.²⁶ Montini and Santo associated bimetallic Pt–Au nanoparticles with reduced anatase nanocrystals, and reported their enhanced activity in the photoreforming of alcohols.^{27,28} Lu and Tong fabricated the reduced TiO₂ nanorods decorated by slight large gold nanoparticles (~5 nm) in a low density.²⁹ These nanorods outperformed TiO₂ and conventional Au/TiO₂ in photochemical water splitting. Both of works exhibit the sign of the synergistic effect between reduced TiO₂ and gold, but they have gold nanoparticles exposed to external environments, which probably causes their aggregation, corrosion and separation from TiO₂. Furthermore, only gold nanoparticles were reviewed in these composites.

Here, the gold nanorods with tunable SPR absorption are encapsulated by a hydrogenated TiO₂ shell (H-TiO₂), which well protects the gold nanorods from external environment. Meanwhile, the H-TiO₂ shell would not shield the light absorbed by the gold nanorods. Such core/shell gold@H-TiO₂ nanorods were achieved by a modified method developed by Wang and Chen,³⁰ where gold nanorods were coated by conventional TiO₂. It is found that Au@H-TiO₂ nanorods show the superior photocatalytic performances to TiO₂, Au@TiO₂ (as-prepared sample), Au@A-TiO₂ (annealed sample in air) in hydrogen evolution, which is attributed to increased light harvesting, enhanced charge separation and reduced charge transfer resistance on the basis of diffused reflection spectra (DRS), transient photocurrent response (TPR), and electro-chemical impedance spectra (EIS).

^aKey Laboratory of Colloid and Interface Chemistry, Ministry of Education, School of Chemistry and Chemical Engineering, Shandong University, Jinan 250100, People's Republic of China. E-mail: yangjian@sdu.edu.cn; Fax: +86-0531-88364489

^bHefei National Laboratory for Physical Sciences at the Microscale, iChEM (Collaborative Innovation Centre of Chemistry for Energy Materials), Hefei Science Centre (CAS), School of Chemistry and Materials Science, University of Science and Technology of China, Hefei, Anhui 230026, P. R. China

† Electronic supplementary information (ESI) available. See DOI: 10.1039/c6ra04444a

Experimental

Materials

$\text{HAuCl}_4 \cdot x\text{H}_2\text{O}$ ($x = 3-5$, Au $\sim 47.8\%$), silver nitrate ($\geq 99.8\%$), sodium borohydride ($\geq 96\%$), ascorbic acid ($\geq 99.7\%$), sodium chloride ($\geq 99.5\%$) and sodium hydrogen carbonate ($\geq 99.5\%$) were purchased from Sinopharm Chemical Reagent Co. Ltd. Cetyltrimethylammonium bromide (CTAB, $\geq 99\%$) was obtained from July Chemical Co. Ltd. Poly(sodium 4-styrenesulfonate) (PSS, MW = 70 000) was ordered from ACROS organics. Titanium(III) chloride (20 wt% TiCl_3 in 3 wt% HCl) was obtained from Alfa Aesar. All the reagents were used without any further purification.

Preparation of PSS wrapped Au nanorods

The high-quality gold nanorods were obtained *via* a typical seed-mediated growth method.^{31,32} 10 mL of the as-obtained solution containing Au nanorods was centrifuged once to remove the excessive surfactants and unreacted reagents. The pellet was then dispersed in 10 mL of distilled water. This solution was added dropwise into an aqueous PSS solution (10 mL, 2 g L^{-1} , containing 6 mM NaCl). After vigorous stirring for 4 h, the PSS-coated Au nanorods were collected by centrifugation and dispersed again in 200 μL of distilled water.

Synthesis of core-shell Au@TiO₂ nanorods

Core-shell Au@TiO₂ nanorods were prepared by a modified method.^{30,33} 200 μL of 17.1 wt% TiCl_3 containing 20 wt% HCl, was diluted by 6 mL of distilled water, followed by the addition of 1.2 mL of 0.93 M NaHCO_3 . Then the PSS-encapsulated Au nanorods were immediately added in the mixture. After the hydrolysis reaction went for 30 min at room temperature, the as-obtained core/shell Au@TiO₂ nanorods were collected by centrifugation twice and then dispersed in 10 mL of water. These nanorods were dried at 60 °C overnight and placed in a tubular furnace. After kept at 450 °C in Ar/H₂ (5% vol) or in air for 2 h, they were cooled naturally and collected for the later use. For the sake of clarity, they were denoted as Au@H-TiO₂ and Au@A-TiO₂.

Characterization

X-ray diffraction (XRD) patterns were obtained from an X-ray powder diffractometer (Bruker D8 Advance, Germany) with monochromatic Cu K α as a radiation source. The working voltage and current of the diffractometer were kept at 40 kV and 40 mA, respectively. Transmission electron microscope (TEM) images were acquired on a transmission electron microscope of JEM-1011 at an accelerating voltage of 100 kV. High-resolution TEM images were recorded on an analytic transmission electron microscope (JEOL 2010, Japan) at 200 kV. Ultraviolet-visible (UV-vis) absorption spectra were obtained at room temperature by a spectrophotometer (Shimadzu UV-2450, Japan). The UV-vis diffuse reflectance spectra (DRS) were measured by a UV-vis spectrometer (Thermal Fisher, Evolution 220) in the range of 300–1000 nm. XPS spectra were achieved on an X-ray

photoelectron Spectrometer (ESCALAB 250) by the internal calibration of the peak of C 1s as 284.6 eV.

Photoelectrochemical measurements

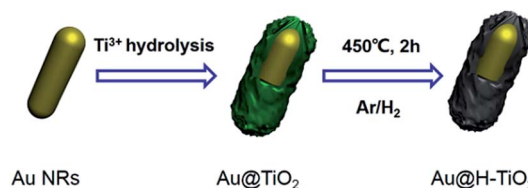
Photoelectrochemical measurements were carried out in a standard three-electrode system. A Pt wire was used as the counter electrode and Ag/AgCl as the reference electrode. To fabricate the photoanode, the ink was prepared by mixing 15 mg of different nanorods and Nafion in ethanol. The ink was then spread on an indium-tin oxide (ITO) conducting glass with an active area about 1.5 cm², and dried under ambient conditions. The electrolyte was a 0.5 M Na_2SO_4 aqueous solution. A 300 W Xe lamp equipped with a UV filter (cut off wavelength, 400 nm) was used as the light source. The photo-currents were measured at 0.5 V with electrochemical station (CHI-760E, China). The electrochemical impedance spectra were acquired from an AUTOLAB PGSTAT204 electrochemical workstation over the frequency range of 100 kHz to 0.01 Hz.

Photocatalytic H₂ generation

2.5 mg of the nanorods was suspended in 10 mL of a mixed solution ($\text{H}_2\text{O} : \text{CH}_3\text{OH} = 1 : 1 \text{ v/v}$) by sonication. The suspension was transferred into a quartz vessel and purged with argon for at least 30 min to drive away dissolved oxygen. After that, the vessel was exposed under a 300 W xenon lamp with a filter (UV cut = 400 nm) to evaluate the photocatalytic activity under visible light. The amount of generated H₂ was determined by gas chromatography (FULI GC-9790II) with a thermal conductivity detector (TCD). In the cycling test, the used nanorods were collected by centrifugation to check its structure stability.

Results and discussion

Scheme 1 shows the synthesis process of core-shell Au@H-TiO₂ nanorods. First, a TiO₂ shell is grown on gold nanorods by the hydrolysis of TiCl_3 at room temperature. Due to molecular oxygen dissolved in the solution, the initial Ti(III) species would be easily oxidized into TiO₂. The slow reaction rate effectively avoids the heterogeneous nucleation of TiO₂ in the bulk solution, thereby facilitating the deposition of TiO₂ on the surface of the gold nanorods (Au@TiO₂). Then, the core-shell Au@TiO₂ nanorods are annealed at 450 °C for 2 h in Ar/H₂, which would result in an enhanced crystallinity for TiO₂ and the appearance of Ti³⁺ in TiO₂. Both of them have been demonstrated to be important to the improvement of the photocatalytic performance of TiO₂.^{30,34,35} Along with the SPR-active gold nanorods at



Scheme 1 Illustration on the formation process of core-shell Au@hydrogenated TiO₂ (Au@H-TiO₂) nanorods.

the core, this nanocomposite (Au@H-TiO₂) successfully combines the SPR material and the photocatalyst within one particle, which allows us to explore the effect of their interaction on the photocatalytic reaction. To disclose the role of Ti³⁺ in the photocatalysis, another batch of the Au@TiO₂ nanorods is annealed in air at 450 °C, denoted as Au@A-TiO₂.

Fig. 1 shows the XRD patterns of Au@TiO₂, Au@A-TiO₂ and Au@H-TiO₂. In the case of Au@TiO₂, only diffraction peaks of gold are observed in the XRD pattern, indicating the amorphous nature of TiO₂ on the gold nanorods. This could be assigned to the low reaction temperature during the hydrolysis reaction. After annealed at a moderate temperature, both Au@H-TiO₂ and Au@A-TiO₂ show the broad diffraction peaks belonging to anatase-phase TiO₂, regardless of the atmosphere. On the basis of Scherrer's formula, the sizes of Au@H-TiO₂ and Au@A-TiO₂ could be estimated as 10.07 and 9.82 nm, very close to each other.

Fig. 2 shows the TEM images of Au@TiO₂, Au@A-TiO₂ and Au@H-TiO₂ nanorods. Compared with the gold nanorods (Fig. S1†), a rough layer of TiO₂ is coated on the surface of gold nanorods (Fig. 2a), which is clearly supported by the size increase of the nanoparticles and the contrast difference between gold and TiO₂. After annealed at a high temperature, the shell thickness of TiO₂ shrinks from 29.4 ± 3.2 nm in Au@TiO₂ to 20.5 ± 2.6 nm in Au@A-TiO₂ or 21.7 ± 3.9 nm in Au@H-TiO₂, although both of them basically keep the rod-like morphology inherited from the gold nanorods (Fig. 2b and c). This shrinkage could be attributed to the releasing of volatile species from amorphous TiO₂ in Au@TiO₂ at a high temperature. This shrinkage also makes the TiO₂ compact, thus probably facilitating the charge transfer during the photocatalysis.^{36,37} HRTEM image (Fig. 2d) shows the clear lattice fringes from anatase TiO₂, confirming its crystalline nature. Furthermore, the thermal treatment causes the decrease of specific surface area (Table S1†), which is probably attributed to the aggregation and surface normalization.

Fig. 3 presents the high-resolution spectra of Ti 2p in Au@TiO₂, Au@A-TiO₂, and Au@H-TiO₂. Compared with the case of Au@TiO₂ and Au@A-TiO₂ (Fig. 3a and b), the doublet of Ti 2p in Au@H-TiO₂ exhibits a tail at the low binding energies,

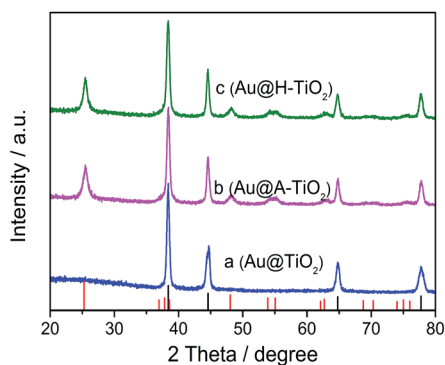


Fig. 1 XRD patterns of as-prepared Au@TiO₂, Au@A-TiO₂ and Au@H-TiO₂. The bottom bars present the standard diffractions of Au (black) and TiO₂ (red).

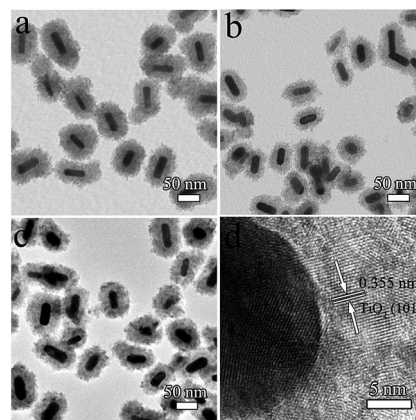


Fig. 2 TEM images of (a) Au@TiO₂, (b) Au@A-TiO₂, and (c) Au@H-TiO₂, and (d) HRTEM images of Au@H-TiO₂.

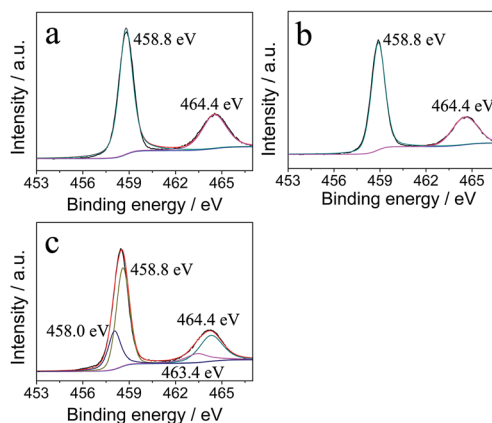


Fig. 3 Ti 2p XPS spectra of (a) Au@TiO₂, (b) Au@A-TiO₂, and (c) Au@H-TiO₂.

which indicates a low valence state of Ti. So, the peaks of Ti 2p_{1/2} and Ti 2p_{3/2} are deconvoluted to get more insights about the information of the low valence state of Ti. As shown in Fig. 3c, the strong peaks at 458.8 and 464.4 eV could be assigned to Ti⁴⁺ from TiO₂,^{20,24,38} also consistent with what observed in Au@TiO₂ (Fig. 3a) and Au@A-TiO₂ (Fig. 3b). The weak peaks at 458.0 and 463.4 eV, are in agreement with those reported for Ti³⁺.^{20,24,38} Moreover, this also demonstrates the presence of oxygen vacancies as it is necessary to maintain electrostatic balance.³⁹ This result is likely caused by the reducing atmosphere during the high-temperature annealing.

Fig. 4a shows the absorption spectra of Au, Au@TiO₂, Au@A-TiO₂, and Au@H-TiO₂ nanorods. Compared with the TSPR and LSPR peaks of the Au nanorods, those of Au@TiO₂ nanorods exhibit significant red-shifts, which could be explained by the change of the dielectric constant around the gold nanorods due to the growth of a TiO₂ shell. As previously reported, the LSPR bands shift to the red with the increasing of medium refractive indexes.⁴⁰ Thus, when the surrounding medium of the gold nanorods change from water (RI = 1.33) to anatase (RI = 2.57), there would be a huge shift in the LSPR band.

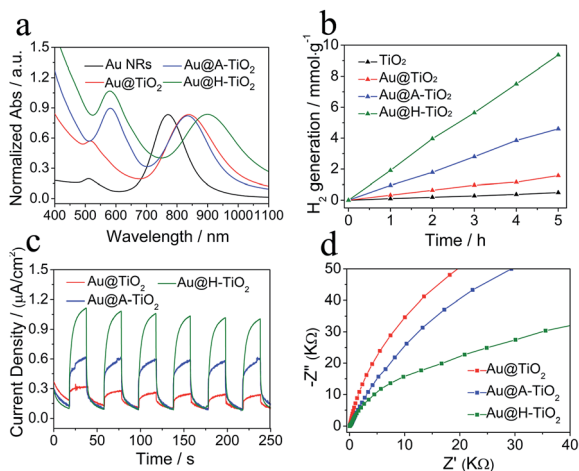


Fig. 4 (a) Absorption spectra of Au, Au@TiO₂, Au@A-TiO₂, and Au@H-TiO₂ nanorods. (b) Production rate of H₂ by different catalysts under visible-light irradiation ($\lambda > 400$ nm). (c) Transient photocurrent densities of different work electrodes with light on/off cycles under visible light irradiation. (d) Nyquist plots of the obtained samples under visible light irradiation.

Since the TiO₂ shells have experienced different treatments in the Au@TiO₂, Au@A-TiO₂, or Au@H-TiO₂ nanorods, they are quite different in terms of their valence states, structures, and crystallinities, thereby inducing different red-shifts.^{30,41} Accordingly, the samples are different in color (Fig. S2†), pink for Au@TiO₂, blue for Au@A-TiO₂, violet for Au@H-TiO₂, meanwhile, the color of the sample powder is darkened after thermal treatment.

The photocatalytic reaction for hydrogen based on the nanorods, is investigated under the irradiation of visible light. It should be noted that these nanorods were directly used as the photocatalysts without the usage of any other cocatalysts. As shown in Fig. 4b, the H₂-generation rate of TiO₂ is only 99.5 $\mu\text{mol h}^{-1} \text{g}^{-1}$. This rate increases to 320.8 $\mu\text{mol h}^{-1} \text{g}^{-1}$ for Au@TiO₂ nanorods, due to enhanced charge separation caused by Au nanorods. After annealing, the rates of H₂ production could be further promoted to 950.8 $\mu\text{mol h}^{-1} \text{g}^{-1}$ for Au@A-TiO₂, indicating the positive contribution of the annealing process on the photocatalytic efficiency. The annealing process could remove absorbed organics/water located on the surface or included into the shell during the hydrolysis of Ti(III) species. Meanwhile, it also promotes the contact and coalescence between neighboring primary particles. Thus, the annealed nanorods (Au@A-TiO₂) would exhibit an enhanced light absorption, a reduced charge recombination and an increased charge-transfer across the interface between electrolyte and electrode, all of which are evidenced by diffused reflection spectra (Fig. S3†), transient photocurrent response (Fig. 4c) and electrochemical impedance spectra (Fig. 4d).

The generation rate of hydrogen arises to 1.912 $\text{mmol h}^{-1} \text{g}^{-1}$ for Au@H-TiO₂, which is much better than those of Au@TiO₂ and Au@A-TiO₂. Compared to Au@A-TiO₂, the superior catalytic activity of Au@H-TiO₂ could be correlated with Ti³⁺ and oxygen vacancies in the H-TiO₂ shell produced in Ar/H₂,

because they were annealed at the same temperature/time. These defects narrow the bandgap and enhance the light absorption,^{42,43} thus improving the catalytic efficiency. Meanwhile, they reduce the charge-transfer resistance, and benefit the charge separation.^{1,23,44–46} These results are supported by diffused reflection spectra (Fig. S3†), transient photocurrent responses (Fig. 4c) and electrochemical impedance spectra (Fig. 4d). In Fig. S3,† Au@H-TiO₂ exhibits the stronger absorption basically over the entire spectra than Au@A-TiO₂, particularly under visible light. Because both of them are quite similar in terms of structures and sizes, the absorption enhancement must come from TiO₂, specifically the Ti³⁺ species and oxygen vacancies in H-TiO₂. It has been reported that these defects could result in a valence band tail, and increase the visible-light absorption,^{20,21} which has been confirmed by XPS spectra, and DFT calculation. Fig. 4c shows the transient photocurrent densities of different nanorods, which could reflect the separation efficiency of photo-excited charges. As noted, Au@H-TiO₂ exhibits a much higher photocurrent density than Au@A-TiO₂, confirming its superior charge-separation efficiency, which is attributed to the presence of Ti³⁺ species and oxygen vacancies. In the EIS spectra (Fig. 4d), all the Nyquist plots under light irradiation display the typical semicircles. But the diameter of the semicircle for Au@H-TiO₂ is smaller than that for Au@A-TiO₂, suggesting its less charge-transfer resistance. These results indicate that the faster transfer and lower recombination of charge carriers in Au@H-TiO₂, consistent with its excellent photocatalytic performance. All these results indicate that the annealing atmosphere is important to the photocatalytic performances of Au@TiO₂.

In order to clarify the SPR effect of Au on the photocatalysis, the gold nanorods are coated by a thin layer of Pd first (Fig. S4a†), then followed by the growth of TiO₂ shell and a thermal treatment in Ar/H₂. Au@Pd@H-TiO₂ nanorods exhibit a similar morphology to that of Au@H-TiO₂ (Fig. 5a). But the Pd shell greatly weakens the SPR bands of the gold nanorods (Fig. S4b†). So, the photocatalysis efficiency caused by the SPR effect should

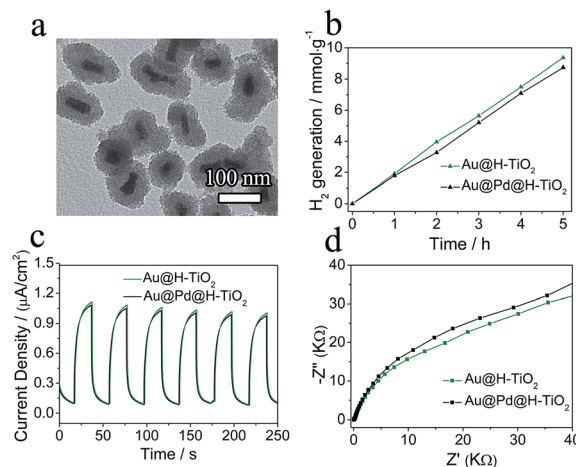


Fig. 5 (a) TEM images of Au@Pd@H-TiO₂ nanorods. (b) Hydrogen generation, (c) transient photocurrent densities, (d) Nyquist plots of Au@H-TiO₂ and Au@Pd@H-TiO₂.

be significantly reduced, if the SPR effect indeed plays a critical role in the reaction. However, as shown in Fig. 5b, there is no obvious difference between Au@H-TiO₂ and Au@Pd@H-TiO₂ nanorods, which is also supported by transient photo-current response (Fig. 5c) and electrochemical impedance spectra (Fig. 5d). These results indicate that the SPR effect on the photocatalysis in our case is negligible. This conclusion can be explained by the limited distance of the SPR effect (Au: ~5 nm) and the thick shell of H-TiO₂ (~20 nm). The effect of the H-TiO₂ shell thickness on photocatalysis also confirms this result. As shown in Fig. S5,† the photocatalytic efficiency of Au@H-TiO₂ increases with the thickness of the H-TiO₂ shell, reflecting the negligible influence of the SPR effect.

In the Au@TiO₂ system, there is a Schottky junction between Au and TiO₂, the excited electrons will transfer from TiO₂ to Au until the two samples attain equilibration, thus separating electron-hole pairs of TiO₂ effectively. Meanwhile, the recombination of electron-holes is retarded and the lifetime of carriers is prolonged. After thermal treatment, especially in hydrogenated atmosphere, the absorption capacity and the migration rate of electrons are improved, which enhance the photocatalytic ability further. The possible electron transfer pathway and reactions on surface for Au@H-TiO₂ are illustrated in Scheme S1.†

The cycling performance of the highest-efficient catalyst, Au@H-TiO₂, is examined under visible light. As presented in Fig. S6,† this is no obvious degradation for the performance of this catalyst, indicating its good stability during the photocatalysis. This conclusion is directly confirmed by the TEM image of this catalyst experienced the photocatalytic reaction (Fig. S7†).

Conclusions

In summary, the core/shell Au nanorod@H-TiO₂ nanorods are successfully synthesized by a controlled hydrolysis reaction followed with a high-temperature annealing. The annealing does not reshape the morphology, but generates Ti³⁺ species along with oxygen vacancies in the shell. At the same time, the crystallinity of the TiO₂ shell is remarkably improved. These nanorods present excellent photocatalytic activities in H₂ generation, higher than TiO₂, Au@TiO₂ and Au@A-TiO₂. Such an enhancement may be attributed to the synergistic effect of Ti³⁺ species, oxygen vacancies and the Au core, which significantly reduce charge recombination and increase charge-transfer across the interface. The effect of surface plasmon resonance of the gold nanorods to the photocatalytic activity is negligible.

Acknowledgements

We want to acknowledge the financial support from the Natural Science Foundation of China (21071055, 21172076 and 21471090), Shandong Provincial Natural Science Foundation for Distinguished Young Scholar (JQ201205), and Taishan Scholarship of Shandong Province (No. ts201511004). The authors thank associate Prof. Di Sun in Shandong University for DRS

measurements, associate Prof. Weiliu Fan in Shandong University for helpful discussion.

References

- 1 G. M. Wang, H. Y. Wang, Y. C. Ling, Y. C. Tang, X. Y. Yang, R. C. Fitzmorris, C. C. Wang, J. Z. Zhang and Y. Li, *Nano Lett.*, 2011, **11**, 3026–3033.
- 2 J. Burschka, N. Pellet, S. J. Moon, R. H. Baker, P. Gao, M. K. Nazeeruddin and M. Gratzel, *Nature*, 2013, **499**, 316–319.
- 3 Y. Ohko, T. Tatsuma, T. Fujii, K. Naoi, C. Niwa, Y. Kubota and A. Fujishima, *Nat. Mater.*, 2003, **2**, 29–31.
- 4 X. L. He, Y. Y. Cai, H. M. Zhang and C. H. Liang, *J. Mater. Chem.*, 2011, **21**, 475–480.
- 5 X. G. Han, Q. Kuang, M. S. Jin, Z. X. Xie and L. S. Zheng, *J. Am. Chem. Soc.*, 2009, **131**, 3152–3153.
- 6 K. Saravanan, K. Ananthanarayanan and P. Balaya, *Energy Environ. Sci.*, 2010, **3**, 939–948.
- 7 V. Etacheri, J. E. Yourey and B. M. Bartlett, *ACS Nano*, 2014, **8**, 1491–1499.
- 8 H. Ren, R. B. Yu, J. Y. Wang, Q. Jin, M. Yang, D. Mao, D. Kisailus, H. J. Zhao and D. Wang, *Nano Lett.*, 2014, **14**, 6679–6684.
- 9 W. J. Youngblood, S. H. A. Lee, Y. Kobayashi, E. A. Hernandez-Pagan, P. G. Hoertz, T. A. Moore, A. L. Moore, D. Gust and T. E. Mallouk, *J. Am. Chem. Soc.*, 2009, **131**, 926–927.
- 10 A. Yella, H. W. Lee, H. N. Tsao, C. Y. Yi, A. K. Chandiran, M. K. Nazeeruddin, E. W. G. Diau, C. Y. Yeh, S. M. Zakeeruddin and M. Grätzel, *Science*, 2011, **334**, 629–634.
- 11 J. B. Sambur and B. A. Parkinson, *ACS Appl. Mater. Interfaces*, 2014, **6**, 21916–21920.
- 12 L. Yang, C. McCue, Q. F. Zhang, E. Uchaker, Y. H. Mai and G. Z. Cao, *Nanoscale*, 2015, **7**, 3173–3180.
- 13 Y. C. Pu, G. M. Wang, K. D. Chang, Y. C. Ling, Y. K. Lin, B. C. Fitzmorris, C. M. Liu, X. H. Lu, Y. X. Tong, J. Z. Zhang, Y. J. Hsu and Y. Li, *Nano Lett.*, 2013, **13**, 3817–3823.
- 14 J. Ohyama, A. Yamamoto, K. Teramura, T. Shishido and T. Tanaka, *ACS Catal.*, 2011, **1**, 187–192.
- 15 J. Du, J. Qi, D. Wang and Z. Y. Tang, *Energy Environ. Sci.*, 2012, **5**, 6914–6918.
- 16 A. Tanaka, Y. Nishino, S. Sakaguchi, T. Yoshikawa, K. Imamura, K. Hashimoto and H. Kominami, *Chem. Commun.*, 2013, **49**, 2551–2553.
- 17 Z. K. Zheng, B. B. Huang, X. D. Meng, J. P. Wang, S. Y. Wang, Z. Z. Lou, Z. Y. Wang, X. Y. Qin, X. Y. Zhang and Y. Dai, *Chem. Commun.*, 2013, **49**, 868–870.
- 18 J. L. Zhang, Y. M. Wu, M. Y. Xing, S. A. K. Leghari and S. Sajjad, *Energy Environ. Sci.*, 2010, **3**, 715–726.
- 19 J. T. Park, W. S. Chi, H. Jeon and J. H. Kim, *Nanoscale*, 2014, **6**, 2718–2729.
- 20 X. B. Chen, L. Liu, P. Y. Yu and S. S. Mao, *Science*, 2011, **331**, 746–750.

- 21 X. B. Chen, L. Liu, Z. Liu, M. A. Marcus, W. C. Wang, N. A. Oyler, M. E. Grass, B. H. Mao, P. A. Glans, P. Y. Yu, J. H. Guo and S. S. Mao, *Sci. Rep.*, 2013, **3**, 1510.
- 22 S. S. Zhang, S. Q. Zhang, B. Y. Peng, H. J. Wang, H. Yu, H. H. Wang and F. Peng, *Electrochem. Commun.*, 2014, **40**, 24–27.
- 23 H. Q. Tan, Z. Zhao, M. Niu, C. Y. Mao, D. P. Cao, D. J. Cheng, P. Y. Feng and Z. C. Sun, *Nanoscale*, 2014, **6**, 10216–10223.
- 24 X. H. Lu, G. M. Wang, T. Zhai, M. H. Yu, J. Y. Gan, Y. X. Tong and Y. Li, *Nano Lett.*, 2012, **12**, 1690–1696.
- 25 T. Xia, W. Zhang, W. J. Li, N. A. Oyler, G. Liu and X. B. Chen, *Nano Energy*, 2013, **2**, 826–835.
- 26 X. Y. Pan and Y. J. Xu, *Appl. Catal., A*, 2013, **459**, 34–40.
- 27 A. Gallo, M. Marelli, R. Psaro, V. Gombac, T. Montini, P. Fornasiero, R. Pievo and V. D. Santo, *Green Chem.*, 2012, **14**, 330–333.
- 28 A. Gallo, T. Montini, M. Marelli, A. Minguzzi, V. Gombac, R. Psaro, P. Fornasiero and V. D. Santo, *ChemSusChem*, 2012, **5**, 1800–1811.
- 29 S. L. Xie, M. Y. Li, W. J. Wei, T. Zhai, P. P. Fang, R. L. Qiu, X. H. Lu and Y. X. Tong, *Nano Energy*, 2014, **10**, 313–321.
- 30 C. H. Fang, H. L. Jia, S. Chang, Q. F. Ruan, P. Wang, T. Chen and J. F. Wang, *Energy Environ. Sci.*, 2014, **7**, 3431–3438.
- 31 B. Nikoobakht and M. A. El-Sayed, *Chem. Mater.*, 2003, **15**, 1957–1962.
- 32 T. K. Sau and C. J. Murphy, *Langmuir*, 2004, **20**, 6414–6420.
- 33 R. Liu and A. Sen, *J. Am. Chem. Soc.*, 2012, **134**, 17505–17512.
- 34 A. S. Wochnik, M. Handloser, D. Durach, A. Hartschuh and C. Scheu, *ACS Appl. Mater. Interfaces*, 2013, **12**, 5696–5699.
- 35 H. Y. Liu, J. B. Joo, M. Dahl, L. S. Fu, Z. Z. Zeng and Y. D. Yin, *Energy Environ. Sci.*, 2015, **8**, 286–296.
- 36 Z. W. Zhang, Y. M. Zhou, Y. W. Zhang, S. M. Xiang, S. J. Zhou and X. L. Sheng, *RSC Adv.*, 2014, **4**, 7313–7320.
- 37 R. J. Dillon, J. B. Joo, F. Zaera, Y. D. Yin and C. J. Bardeen, *Phys. Chem. Chem. Phys.*, 2013, **15**, 1488–1496.
- 38 M. S. Lazarus and T. K. Sham, *Chem. Phys. Lett.*, 1982, **92**, 670–674.
- 39 X. D. Jiang, Y. P. Zhang, J. Jiang, Y. S. Rong, Y. C. Wang, Y. C. Wu and C. X. Pan, *J. Phys. Chem. C*, 2012, **116**, 22619–22624.
- 40 J. Yang, *et al.*, *Chem. Phys. Lett.*, 2005, **416**, 215–219.
- 41 W. L. Liu, F. C. Lin, Y. C. Yang, C. H. Huang, S. Gwo, M. H. Huang and J. S. Huang, *Nanoscale*, 2013, **5**, 7953–7962.
- 42 J. Tian, Y. H. Leng, Z. H. Zhao, Y. Xia, Y. H. Sang, P. Hao, J. Zhan, M. C. Li and H. Liu, *Nano Energy*, 2015, **11**, 419–427.
- 43 Z. Wang, C. Y. Yang, T. Q. Lin, H. Yin, P. Chen, D. Y. Wan, F. F. Xu, F. Q. Huang, J. H. Lin, X. M. Xie and M. H. Jiang, *Adv. Funct. Mater.*, 2013, **23**, 5444–5450.
- 44 X. Y. Pan, M. Q. Yang, X. Z. Fu, N. Zhang and Y. J. Xu, *Nanoscale*, 2013, **5**, 3601–3614.
- 45 Z. K. Zheng, B. B. Huang, J. B. Lu, Z. Y. Wang, X. Y. Qin, X. Y. Zhang, Y. Dai and M. H. Whangbo, *Chem. Commun.*, 2012, **48**, 5733–5735.
- 46 J. C. Huo, Y. J. Hu, H. Jiang and C. Z. Li, *Nanoscale*, 2014, **6**, 9078–9084.